Evaluating Beam Smoothing Techniques in Laser-Driven Inertial Confinement Fusion Using Spatial-Frequency Power Spectral Density of Focal-Spot-Intensity Relative Deviation*

Chuanchao Zhang(张传超)†, Baoshen Jia(贾宝申), Fa Zeng(曾发)†, Wei Liao(廖威), Xiaolong Jiang(蒋晓龙), Wei Ni (倪卫) , Xiaodong Jiang(蒋晓东), Ping Li(李平) and Qihua Zhu(朱启华)

Laser Fusion Research Center, China Academy of Engineering Physics, Mianyang 621900, China

We propose an evaluation approach based on spatial-frequency power spectral density of focal-spot-intensity relative deviation (PSDFRD), which corresponds to the spatial frequency distribution of squared focal-spot-intensity contrast, to quantify the effectiveness of beam smoothing techniques in laser-driven inertial confinement fusion (ICF). This approach enables assessment of smoothing effects that cannot be adequately distinguished by conventional metrics like contrast and fractional power above intensity (FOPAI). Beam smoothing techniques employed in this work include continuous phase plate (CPP), smoothing by spectral dispersion (SSD), and polarization smoothing (PS) with two implementations: birefringent wedge (BW) and spatially-random polarization control plate (SRPCP)). Focal spot intensity distributions were characterized for six beam smoothing configurations (CPP only, CPP+BW, CPP+SRPCP, CPP+SSD, CPP+BW+SSD, and CPP+SRPCP+SSD), with uniformity analyzed using the proposed method. CPP+PS (BW or SRPCP) configurations enhance intensity distribution and improve uniformity in the low-frequency range (0–0.002 μm^{-1}), but introduce increased intensity and non-uniformity at high frequencies (0.050–0.070 μm^{-1}). Compared to the one-dimensionally periodic smoothing characteristics of CPP+BW across spatial frequencies, CPP+SRPCP demonstrates superior smoothing uniformity across all spatial frequency domains. CPP+SSD reduces intensity distribution and improves uniformity across most frequencies, but it significantly increases both intensity and non-uniformity in the low-frequency region (0-0.001 μm^{-1}). The CPP+PS (BW or SRPCP) +SSD not only mitigates elevated high-frequency intensity and non-uniformity inherent to the CPP+PS (BW or SRPCP) but also reduces low-frequency non-uniformity characteristic of CPP+SSD. Therefore, the combination of CPP, PS, and SSD exhibits a complementary smoothing effect.

Keywords: beam smoothing, power spectral density, continuous phase plate, smoothing by spectral dispersion, polarization smoothing

PACS: 42.70.Ce, 61.80.–x, 63.50.–x, 78.20.–e

* Project supported by National Natural Science Foundation of China (Grant No. 62275235).
† Corresponding author. E-mail: zhchch@caep.cn
† Corresponding author. E-mail: cengfa@tsinghua.org.cn

1. Introduction

Beam smoothing techniques, such as continuous phase plate (CPP),[1-4] smoothing by spectral dispersion (SSD),[5,6] and polarization smoothing (PS),[9-11] are widely employed in most high-power laser facilities for inertial confinement fusion (ICF). CPP governs the global envelope of the focal spot while eliminating large-scale intensity modulation. SSD suppresses interference speckles at medium-to-high spatial frequencies through temporal averaging effects. PS enables instantaneous superposition of two incoherent beams via the polarization dimension without temporal integration, proving essential for suppressing ultrafast laser-plasma instabilities. These beam smoothing techniques have been implemented to collectively minimize laser focal spot non-uniformity, thereby achieving high hohlraum coupling efficiency, superior radiation symmetry, and robust implosion stability, which directly support the attainment of ignition conditions for self-sustaining fusion burn. [12-21]

Conventional metrics for evaluating focal spot uniformity induced by beam smoothing techniques include contrast and fractional power above intensity (FOPAI).[4,22] While simple and effective, these metrics quantify intensity magnitude alone without spatial-frequency distribution data. Critically, non-uniformity at different spatial frequencies causes distinct harmful effects: low-frequency non-uniformity induces Rayleigh-Taylor instabilities, while high-frequency non-uniformity drives laser-plasma instabilities. Consequently, the power spectral density (PSD) of focal spot intensities is used to assesses smoothing performance.[4,22] However, PSD of focal spot intensities cannot be directly correlated with conventional metrics, making quantitative comparisons difficult.

An evaluation approach based on the spatial-frequency power spectral density of focal-spot-intensity relative deviation (PSDFRD), which corresponds to the spatial frequency distribution of the square of focal spot contrast, was explored to characterize beam smoothing effectiveness. In this study, two PS techniques, birefringent wedge (BW) and spatially-random polarization control plate (SRPCP),[9,10] were used. Uniformity analysis using the PSDFRD method was performed on focal spots for six beam smoothing configurations: CPP only, CPP+BW, CPP+SRPCP, CPP+SSD, CPP+BW+SSD, and CPP+SRPCP+SSD. The PSDFRD approach quantitatively characterizes focal spot uniformity variations across spatial frequencies in each configuration.

2. Theory

The non-uniformity of focal spot intensity $I(x,y)$ appears as fluctuations about the average intensity. Generally, the non-uniformity of focal spot intensity $I(x,y)$ is calculated only in the selected central region S in the focal plane. Thus, we create a window function $W(x,y)$ that is zero outside S and one inside S. The window function adopted for PSDFRD analysis is consistent with that utilized in focal spot contrast assessment. The area of the selected central region S can be calculated by

$$A=\iint_S W(x,y)\mathrm{d}x\mathrm{d}y=\int_{-L_x/2}^{L_x/2}\int_{-L_y/2}^{L_y/2}W(x,y)\mathrm{d}x\mathrm{d}y\,. \qquad (1)$$

The average intensity of focal spot in the selected central region S is given by

$$I_{S_\mathrm{mean}} = \frac{1}{A}\iint_S I(x,y)\mathrm{d}x\mathrm{d}y = \frac{1}{A}\int_{-\mathrm{L_x}/2}^{\mathrm{L_x}/2}\int_{-\mathrm{L_y}/2}^{\mathrm{L_y}/2} I(x,y)W(x,y)\mathrm{d}x\mathrm{d}y \qquad (2)$$

To quantify the level of non-uniformity in the selected central region S of focal spot, the mean square of focal-spot-intensity relative deviation (σ_{rms}^2) can be written in the form as

$$\begin{aligned}\sigma_{\mathrm{rms}}^2 &= \frac{1}{A}\iint_S \frac{[I(x,y)-I_{S_\mathrm{mean}}]^2}{I_{S_\mathrm{mean}}^2}\mathrm{d}x\mathrm{d}y \\ &= \frac{1}{A}\int_{-\mathrm{L_x}/2}^{\mathrm{L_x}/2}\int_{-\mathrm{L_y}/2}^{\mathrm{L_y}/2}\frac{[I(x,y)-I_{S_\mathrm{mean}}]^2}{I_{S_\mathrm{mean}}^2}W^2(x,y)\mathrm{d}x\mathrm{d}y\end{aligned} \qquad (3)$$

The root mean square of focal-spot-intensity relative deviations (σ_{rms}) is the contrast of focal spot intensities in the selected central region S. We define the normalized relative deviation from the average intensity in the selected central region S at the position of (x,y) in the form as

$$\sigma(x,y) = \frac{1}{\sqrt{A}}\frac{I(x,y)-I_{S_\mathrm{mean}}}{I_{S_\mathrm{mean}}}W(x,y) \qquad (4)$$

Then, the relation (3) can be written as

$$\sigma_{\mathrm{rms}}^2 = \iint \sigma^2(x,y)\mathrm{d}x\mathrm{d}y \qquad (5)$$

From Parseval's theorem,

$$\sigma_{\mathrm{rms}}^2 = \iint \sigma^2(x,y)\mathrm{d}x\mathrm{d}y = \iint \left|\sigma_f(f_x,f_y)\right|^2 \mathrm{d}f_x\mathrm{d}f_y \qquad (6)$$

Where, the $\sigma_f(f_x,f_y)$ is the Fourier transform of $\sigma(x,y)$,

$$\sigma_f(f_x,f_y) = \iint \sigma(x,y)\exp[-\mathrm{j}2\pi(f_x x+f_y y)]\,\mathrm{d}x\,\mathrm{d}y \qquad (7)$$

The $\left|\sigma_f(f_x,f_y)\right|^2$ is the two-dimensional PSDFRD, and characterizes the contribution to the non-uniformity σ_{rms}^2 of focal spot intensities at the spatial frequency of (f_x,f_y).

Generally, focal spot intensities are measured using a far-field CCD camera with M×N pixels, where the pixel size is defined as Δx×Δy. To quantify focal spot intensity non-uniformity at specific spatial frequencies using discrete-signal far-field CCD images, the aforementioned relations 1-7 require discretization.

The sampling points N_S in the selected central region S can be calculated by

$$N_S = \sum_{m=0}^{\mathrm{M}-1}\sum_{n=0}^{\mathrm{N}-1} W(m,n), \qquad (8)$$

where, $m = 0,1,2,\ldots,\mathrm{M}-1$, and $n = 0,1,2,\ldots,\mathrm{N}-1$.

The average intensity I_{S_mean} of focal spot in the selected central region S is discretely given by

$$I_{S_\mathrm{mean}} = \frac{1}{N_S}\sum_{m=0}^{\mathrm{M-1}}\sum_{n=0}^{\mathrm{N-1}} I(m,n)W(m,n) \qquad (9)$$

The non-uniformity σ_{rms}^2 of focal spot intensities in the selected central region S can be discretely written in the form as

$$\sigma_{\mathrm{rms}}^2 = \frac{1}{N_S}\sum_{m=0}^{\mathrm{M-1}}\sum_{n=0}^{\mathrm{N-1}} \frac{[I(m,n)-I_{S_\mathrm{mean}}]^2}{I_{S_\mathrm{mean}}^2} W^2(m,n) \qquad (10)$$

The normalized relative deviation from the average intensity in the selected central region S can be discretely given in the form as

$$\sigma(m,n) = \frac{1}{\sqrt{N_S}} \frac{I(m,n)-I_{S_\mathrm{mean}}}{I_{S_\mathrm{mean}}} W(m,n) \qquad (11)$$

Then, the Fourier transform of $\sigma(m,n)$ can be calculated by

$$\sigma_f(k,l) = \sum_{m=0}^{\mathrm{M-1}}\sum_{n=0}^{\mathrm{N-1}} \sigma(m,n)\exp[-\mathrm{j}2\pi(\frac{mk}{\mathrm{M}}+\frac{nl}{\mathrm{N}})], \qquad (12)$$

where, $k = 0,1,2,\ldots,\mathrm{M}-1$, and $l = 0,1,2,\ldots,\mathrm{N}-1$.

Therefore, from Parseval's theorem, the σ_{rms}^2 of focal spot intensities can be discretely written in the form as

$$\sigma_{\mathrm{rms}}^2 = \sum_{m=0}^{\mathrm{M-1}}\sum_{n=0}^{\mathrm{N-1}} \sigma^2(m,n) = \frac{1}{\mathrm{MN}}\sum_{k=0}^{\mathrm{M-1}}\sum_{l=0}^{\mathrm{N-1}} \left|\sigma_f(k,l)\right|^2 \qquad (13)$$

We define the normalized two-dimensional PSDFRD contributing to the non-uniformity σ_{rms}^2 of relative focal spot intensity at the spatial frequency of (f_{x_k}, f_{y_l}) in the form as

$$PSDFRD(f_{x_k}, f_{y_l}) = \frac{1}{\mathrm{MN}} \frac{\left|\sigma_f(k,l)\right|^2}{\Delta f_x \Delta f_y}, \qquad (14)$$

where, $f_{x_k} = k/(\mathrm{M}\Delta x)$, $f_{y_l} = l/(\mathrm{N}\Delta y)$, $\Delta f_x = 1/(\mathrm{M}\Delta x)$ and $\Delta f_y = 1/(\mathrm{N}\Delta y)$.

Thus, the non-uniformity σ_{rms}^2 of focal spot intensities in the selected central region S can be written as

$$\sigma_{\mathrm{rms}}^2 = \sum_{k=0}^{\mathrm{M-1}}\sum_{l=0}^{\mathrm{N-1}} PSDFRD(f_{x_k}, f_{y_l})\Delta f_x \Delta f_y \qquad (15)$$

3. Experimental

A 351 nm laser beam with a 385 mm × 385 mm square aperture was used in the experiments. After passing through a CPP, the laser beam was focused by a 12 m focal-length lens to produce a circular 700 μm-diameter focal spot. The one-dimensional SSD employed an infrared bandwidths of 0.30nm with 19.9 GHz modulator.[4] PS implemented two optional techniques: BW and SRPCP. The BW, fabricated from KDP crystals, split the incident 351 nm light into two orthogonally polarized beams of equal power with a slight angular separation. This component was positioned upstream of the CPP.[9] After traversing the BW and CPP, the laser beam

generated two speckle patterns displaced by 130 μm through lens focusing. The SRPCP, fabricated from fused silica, transformed the incident 351 nm light into an emerging beam exhibiting a spatially random polarization distribution.[10] Focal spot intensities for six beam smoothing configurations: CPP only, CPP+BW, CPP+SRPCP, CPP+SSD, CPP+BW+SSD, and CPP+SRPCP+SSD, were measured using a far-field low dark current and noise CCD camera with 3.75 μm resolution.

4. Results and discussion

4.1. Contrast and FOPAI of focal spots

A specific beam smoothing configuration determines its corresponding beam smoothing effect. Fig. 1 shows the typical measured intensity distributions of focal spots for six configurations: CPP only, CPP+BW, CPP+SRPCP, CPP+SSD, CPP+BW+SSD, and CPP+SRPCP+SSD. Compared to CPP only (Fig. 1(a)), adding BW or SRPCP significantly refined the speckle grains and enhanced uniformity of the focal spot (Figs. 1(b) and 1(c)). The mechanism of PS operates through depolarization of the linearly polarized near-field beam via polarization control elements (e.g., BW and SRPCP), which converts partial beam energy into an orthogonal polarization state relative to the incident beam. Consequently, the resulting focal spot manifests as an incoherent superposition of two orthogonally polarized components. Therefore, coarse, sparse speckle grains without polarization smoothing are markedly converted into fine, fragmented speckle grains with polarization smoothing,

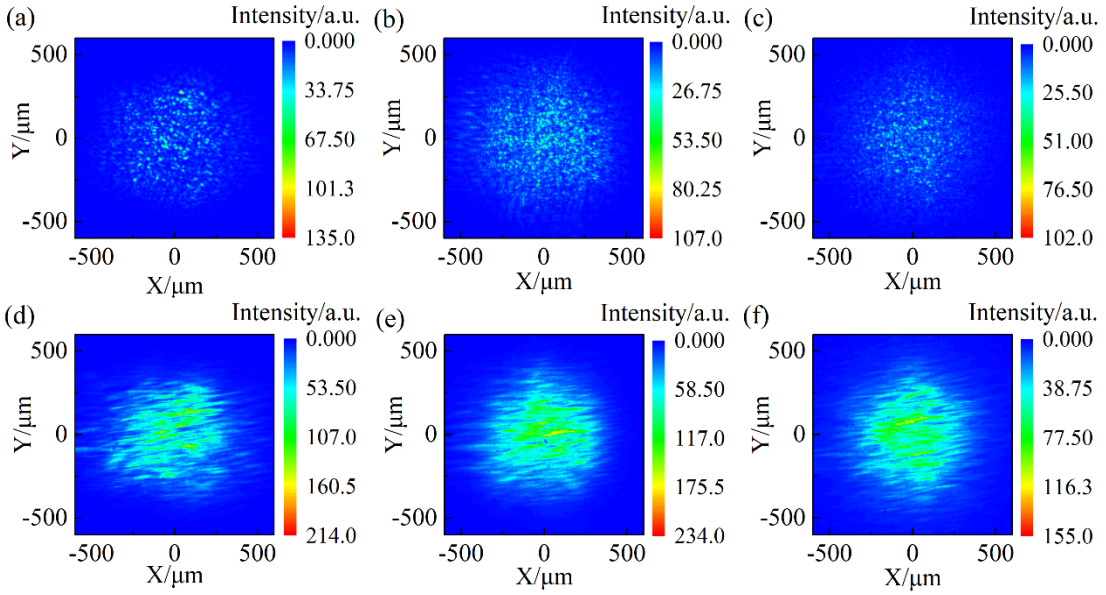


Fig. 1. (colour online) Measured intensity distributions of focal spots for six configurations: (a) CPP only, (b) CPP+BW, (c) CPP+SRPCP, (d) CPP+SSD, (e) CPP+BW+SSD, and (f) CPP+SRPCP+SSD.

With further addition of SSD, the focal spot was further homogenized. SSD reduces focal spot non-uniformity through temporal integration. A characteristic phenomenon involves spatial scanning of the focal spot in a specific direction over time, as illustrated in Fig. 1(d), (e), and (f), where horizontal sweeping is observed, which effectively suppresses high-frequency speckles. However, the scanning generates a striped focal spot distribution, yielding limited improvement or even degradation in

low-frequency uniformity.

Contrast is commonly used to characterize the uniformity of the focal spot, and its mathematical definition is given by

$$Contrast = \sqrt{\frac{\iint_S [I(x,y) - I_{\text{mean}}]^2 \,\mathrm{d}x\,\mathrm{d}y}{\iint_S I_{\text{mean}}^2 \,\mathrm{d}x\,\mathrm{d}y}}. \qquad (16)$$

Where S is the focal spot area, and I_{mean} is the average intensity in S. According to Eqs. (3), (13) and (14), the contrast is equal to the root mean square of focal-spot-intensity relative deviation (σ_{rms}), and the PSDFRD quantifies the contribution to the squared contrast of focal spot at the spatial frequency of (f_x, f_y).

The contrast in the central 700 μm diameter area of the focal spot was calculated for each configurations. The values are: 1.08 for CPP only, 0.79 for CPP+BW, 0.79 for CPP+SRPCP, 0.60 for CPP+SSD, 0.52 for CPP+BW+SSD, and 0.50 for CPP+SRPCP+SSD. Compared to the CPP-only case (1.08), the contrast reduces to approximately 0.73 for CPP+BW and CPP+SRPCP, 0.56 for CPP+SSD, 0.48 for CPP+BW+SSD, and 0.46 for CPP+SRPCP+SSD. For the configurations, both BW and SRPCP reduce the contrast to about 0.71 times the theoretical value. Adding SSD further reduces it below 0.5. Therefore, based solely on contrast, it is impossible to distinguish between the CPP+BW and CPP+SRPCP configurations or determine the superiority of CPP+BW+SSD versus CPP+SRPCP+SSD.

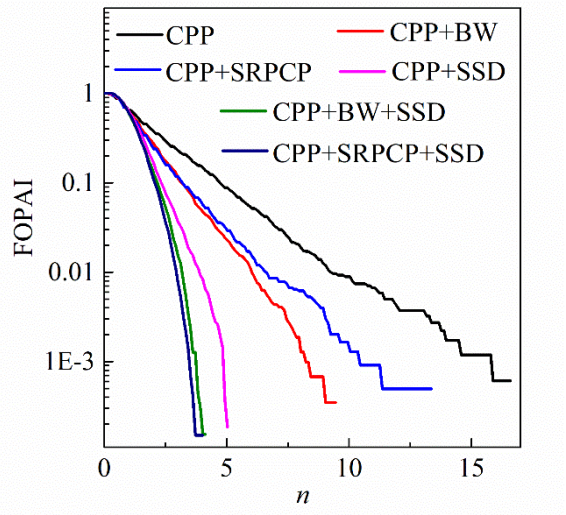


Fig. 2. (colour online) FOPAI curves for six configurations: CPP only, CPP+BW, CPP+SRPCP, CPP+SSD, CPP+BW+SSD, and CPP+SRPCP+SSD. These curves were calculated using intensities from a central 700-μm-diameter region of the focal spots.

Another common metric for evaluating focal spot smoothing is the fraction of power above n times the average intensity (FOPAI(n)), which accounts for high-intensity speckle distribution effects. FOPAI(n) is defined as

$$FOPAI(n) = \frac{\iint_{S(I(x,y)>nI_{\text{mean}})} I(x,y)\,\mathrm{d}x\,\mathrm{d}y}{\iint_S I(x,y)\,\mathrm{d}x\,\mathrm{d}y}. \qquad (17)$$

As shown in Fig. 2, the FOPAI curve clearly demonstrates significant suppression of high-intensity speckle energy after introducing BW or SRPCP. The fraction of power above $5\times I_{mean}$ (FOPAI(5)) is 8.8% for CPP only. With BW or SRPCP, this fraction drops to 2.3% for CPP+BW and 2.9% for CPP+SRPCP. The FOPAI(5) value for CPP+SRPCP is slightly higher than for CPP+BW. After further adding SSD, FOPAI(5) reduces to zero in all cases. The FOPAI curves of CPP+SRPCP+SSD and CPP+BW+SSD are nearly identical. While FOPAI quantifies the energy proportion of high-energy speckles, it cannot reveal their spatial distribution or distinguish smoothing schemes with similar FOPAI profiles.

4.2. Two-dimensional PSDFRD

Fig. 3 presents the two-dimensional PSDFRD for six configurations: CPP only, CPP+BW, CPP+SRPCP, CPP+SSD, CPP+BW+SSD, and CPP+SRPCP+SSD. The CPP+BW configuration exhibits characteristic periodic reduction in PSDFRD (Fig. 3(b)), with a maximum value of 6124 μm², indicating a 37% reduction from the CPP-only baseline of 9687 μm². In contrast, CPP+SRPCP demonstrates nearly uniform reduction across all spatial frequencies, with a maximum value of 4191 μm², representing a 57% reduction from the baseline. Although both configurations achieve identical contrast levels, their PSDFRD distributions are fundamentally distinct: CPP+SRPCP reduces values uniformly across spatial frequencies, while CPP+BW produces localized periodic reduction. Consequently, CPP+SRPCP achieves superior focal spot smoothing compared to CPP+BW.

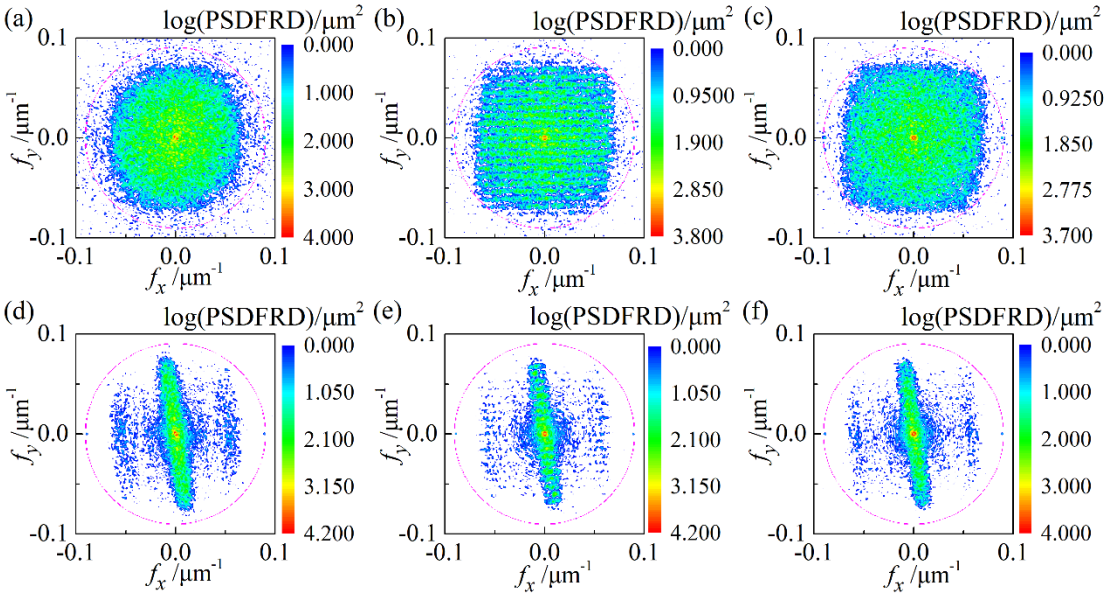


Fig. 3. (colour online) The two-dimensional PSDFRD for six configurations: (a) CPP only, (b) CPP+BW, (c) CPP+SRPCP, (d) CPP+SSD, (e) CPP+BW+SSD, and (f) CPP+SRPCP+SSD. Intensity values from a central 700-μm-diameter region of the focal spots were used for each PSDFRD calculation. A pink ring marks the spatial frequency corresponding to the speckle size.

With the addition of SSD (in configurations such as CPP+SSD, CPP+BW+SSD, and CPP+SRPCP+SSD), PSDFRD decreases at most spatial frequencies while retaining only the distribution near the f_y-axis, but the maximum PSDFRD value increases. For CPP+SSD, the maximum PSDFRD value increases to 15490 μm², representing a 60%

rise relative to CPP only (Fig. 3(d)). For CPP+BW+SSD, PSDFRD combines features of both CPP+BW and CPP+SSD while preserving a periodic distribution near the f_y-axis, with a maximum value of 13301 μm² corresponding to a 37% increase over CPP only (Fig. 3(e)). For CPP+SRPCP+SSD, PSDFRD combines features of both CPP+SRPCP and CPP+SSD, with a maximum value of 8688 μm², representing a 10% increase over CPP only (Fig. 3(f)). Clearly, for CPP+BW+SSD and CPP+SRPCP+SSD, which are difficult to distinguish using traditional focal spot uniformity metrics like contrast and FOPAI, PSDFRD can reveal their fine distinctions.

4.3. One-dimensional PSDFRD

To quantify focal spot intensity non-uniformities more visually, one-dimensional PSDFRD in orthogonal directions were derived from the two-dimensional PSDFRD, defined as

$$\begin{aligned} PSDFRD(f_x) &= \int PSDFRD(f_x, f_y)\mathrm{d}f_y \\ PSDFRD(f_y) &= \int PSDFRD(f_x, f_y)\mathrm{d}f_x \end{aligned} . \qquad (18)$$

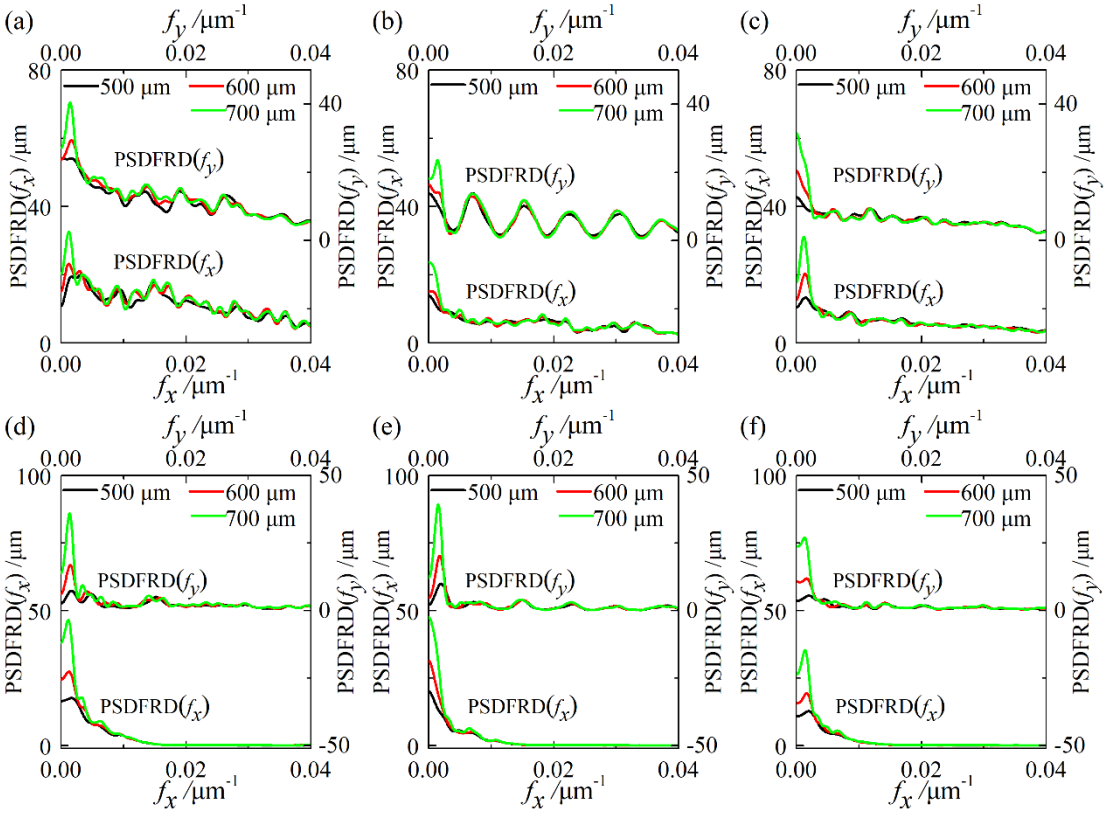


Fig.4. The one-dimensional PSDFRD(f_x) and PSDFRD(f_y) for the CPP only (a), CPP+BW (b), CPP+SRPCP (c), CPP+SSD (d), CPP+BW+SSD (e), and CPP+SRPCP+SSD (f) configurations. Intensity values from central regions of the focal spots with 500 μm, 600 μm, and 700 μm diameters were used for each PSDFRD(f_x) and PSDFRD(f_y) calculation.

To quantitatively assess the influence of uniformity results to the choice of the central region size of focal spots, the orthogonal one-dimensional PSDFRD(f_x) and PSDFRD(f_y) were systematically calculated for six beam smoothing configurations, utilizing the focal spot images from Fig. 1. Varying circular window function sizes

with diameters of 500 μm, 600 μm, and 700 μm are applied to investigate the influence of varying window function sizes on the PSDFRD. Fig. 4 shows the one-dimensional PSDFRD(f_x) and PSDFRD(f_y) calculated from intensity values from central regions of the focal spots with different diameters of 500 μm, 600 μm, and 700 μm. The influence of varying window function sizes on the PSDFRD, demonstrating no discernible spectral leakage transfer to the sidelobes, which indicates that circular window functions can be effectively applied to PSDFRD analysis.

It is evident from Fig.4 that for all configurations, when the selected central region size within the 500–700 μm range, the central region size primarily affect PSDFRD(f_x) and PSDFRD(f_y) values exclusively in the low spatial frequency domain (0–0.003 μm^{-1}). The PSDFRD(f_x) and PSDFRD(f_y) values at higher spatial frequencies remain virtually unchanged. Within the low-frequency range (0–0.003 μm^{-1}), smaller central region dimensions correspond to reduced PSDFRD(f_x) and PSDFRD(f_y) values, thus indicating enhanced uniformity near the focal spot center at low spatial frequencies. Therefore, PSDFRD can precisely quantify the influence of selected focal spot central region size on the uniformity results.

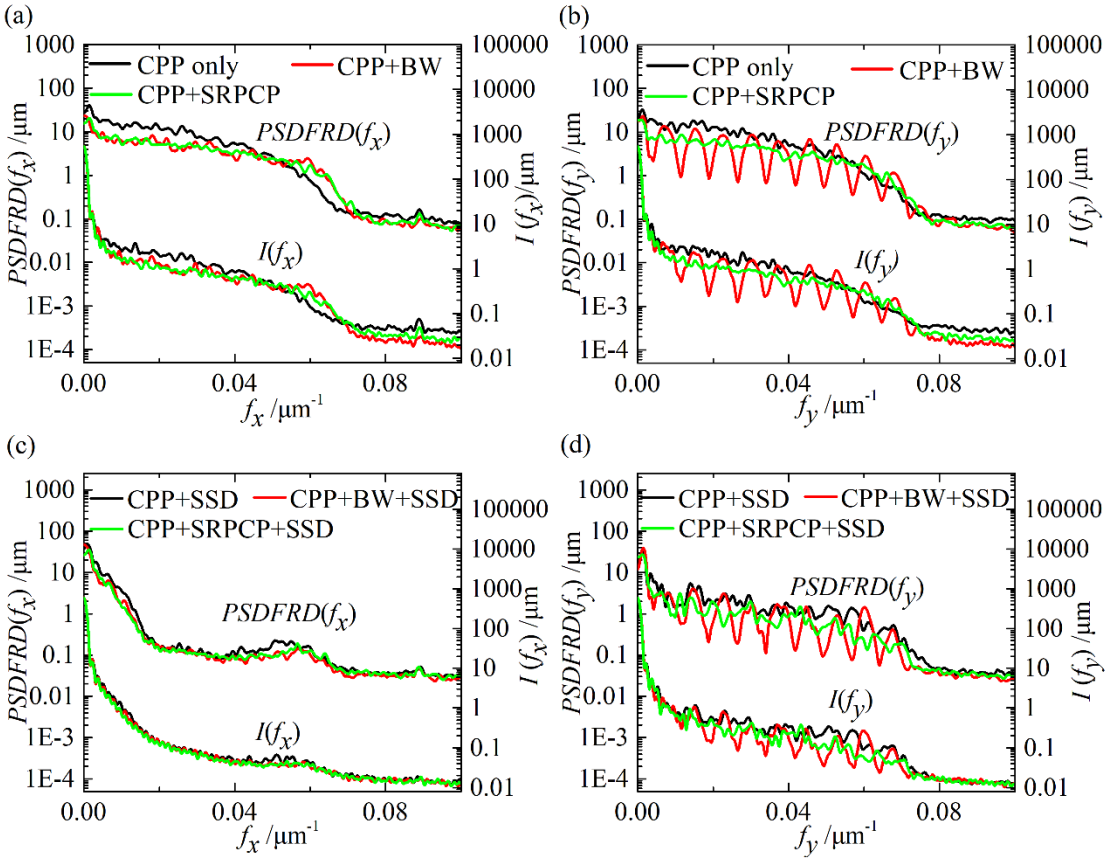


Fig. 5. (colour online) The one-dimensional $PSDFRD(f_x)$ (a) and $PSDFRD(f_y)$ (b) for the CPP-only, CPP+BW, and CPP+SRPCP configurations. Similarly, $PSDFRD(f_x)$ (c) and $PSDFRD(f_y)$ (d) for the CPP+SSD, CPP+BW+SSD, and CPP+SRPCP+SSD configurations. The corresponding one-dimensional intensity distributions $I(f_x)$ and $I(f_y)$ are also plotted in each figure

To evaluate the uniformity within the concerned 700 μm diameter central region of focal spots across various configurations, we computed and present the corresponding

one-dimensional PSDFRD for all configurations in Fig. 5 using the two-dimensional PSDFRD data in Fig. 3. Comparatively, the spatial frequency distributions of one-dimensional focal spot intensity $I(f_x)$ and $I(f_y)$ are co-plotted in Fig. 5.

Along the f_x direction, both CPP+BW and CPP+SRPCP exhibit reduced $PSDFRD(f_x)$ values relative to CPP only across most spatial frequencies, accompanied by decreased $I(f_x)$, as shown in Fig. 5(a). Notably, however, anomalous variations emerge in the low-frequency (0–0.002 μm^{-1}) and high-frequency (0.050–0.070 μm^{-1}) regions. Within the low-frequency range, $PSDFRD(f_x)$ decreases for both CPP+BW and CPP+SRPCP, whereas $I(f_x)$ increases, which indicates that applying both CPP+BW and CPP+SRPCP enhances focal spot energy and improves uniformity in the low-frequency region along the f_x direction. Conversely, in the high-frequency region, $PSDFRD(f_x)$ increases alongside elevated $I(f_x)$ values, which means that achieving a uniform flat-top focal spot in the spatial domain requires added high-frequency components in the spatial frequency domain, as dictated by Fourier transform principles.

Along the f_y direction, CPP+SRPCP exhibits trends in $PSDFRD(f_y)$ and $I(f_y)$ largely consistent with its $PSDFRD(f_x)$ and $I(f_x)$ behavior, indicating isotropic focal spot smoothing, as shown in Fig. 5(b). Conversely, CPP+BW demonstrates significant periodicity in in $PSDFRD(f_y)$ and $I(f_y)$: effective smoothing occurs at spectral troughs, while peak regions exhibit degraded or non-uniform smoothing. Thus, CPP+BW exhibits anisotropic focal spot smoothing, demonstrating effectiveness only at part spatial frequencies along the f_y direction.

With the additional integration of SSD, $PSDFRD(f_x)$ values for all configurations exhibit significant reduction across most spatial frequencies along the f_x direction. Along the f_y direction, $PSDFRD(f_y)$ values also decrease but show a smaller magnitude of reduction compared to $PSDFRD(f_x)$, attributable to the one-dimensional nature of the implemented SSD, as evidenced in Fig. 5(b) and (c). Collectively, these one-dimensional PSDFRD profiles confirm that combined smoothing techniques yield additive smoothing effects.

For comparison, the conventional one-dimensional PSD(f_x) and PSD(f_y) are presented in Fig. 6. A comparison of Figs. 5 and 6 clearly reveals the distinction between PSD and PSDFRD. PSD is normalized using a manually selected peak at zero spatial frequency, demonstrating relative variations in the spatial frequency distribution of focal spot intensity power, and cannot be correlated with the contrast parameter characterizing focal spot uniformity. Moreover, due to normalization at the zero-frequency peak, PSD cannot assess uniformity at zero frequency. In contrast, PSDFRD directly provides a quantitative spatial frequency distribution of the square of focal spot intensity contrast, intuitively indicating the degree of deviation from the mean at each spatial frequency, thereby enabling high-quality evaluation of focal spot uniformity. Therefore, compared to conventional PSD, the PSDFRD proposed in this study cannot be regarded as merely a reformulation but possesses deeper physical significance, and is of significant importance for evaluating existing beam smoothing techniques and advancing beam smoothing technology.

For comparison, the conventional one-dimensional PSD(f_x) and PSD(f_y) are presented

in Fig. 6. A comparison of Figs. 5 and 6 clearly reveals the distinction between PSD and PSDFRD. PSD is normalized using a manually selected peak at zero spatial frequency, demonstrating relative variations in the spatial frequency distribution of focal spot intensity power, and cannot be correlated with the contrast parameter characterizing focal spot uniformity. Moreover, due to normalization at the zero-frequency peak, PSD cannot assess uniformity at zero frequency. In contrast, PSDFRD directly provides a quantitative spatial frequency distribution of the square of focal spot intensity contrast, intuitively indicating the degree of deviation from the mean at each spatial frequency, thereby enabling high-quality evaluation of focal spot uniformity. Therefore, compared to conventional PSD, the PSDFRD proposed in this study cannot be regarded as merely a reformulation but possesses deeper physical significance, and is of significant importance for evaluating existing beam smoothing techniques and advancing beam smoothing technology.

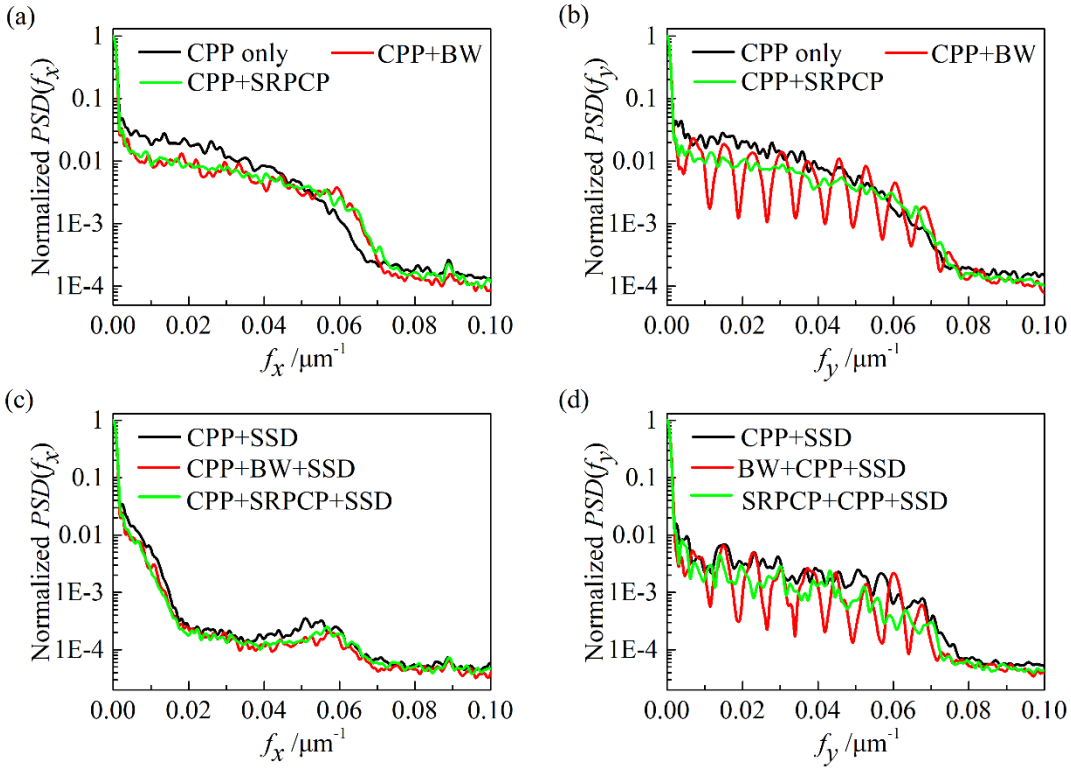


Fig. 6. (colour online) The conventional normalized one-dimensional $PSD(f_x)$ (a) and $PSD(f_y)$ (b) for the CPP-only, CPP+BW, and CPP+SRPCP configurations. Similarly, $PSD(f_x)$ (c) and $PSD(f_y)$ (d) for the CPP+SSD, CPP+BW+SSD, and CPP+SRPCP+SSD configurations.

For enhanced observation of focal spot uniformity and intensity variations across spatial frequencies, we normalized the one-dimensional PSDFRD and intensity values for CPP+BW, CPP+SRPCP, CPP+SSD, CPP+BW+SSD, and CPP+SRPCP+SSD configurations by computing their relative values to the CCP-only baseline at each frequency. The resultant relative PSDFRD and intensity distributions versus spatial frequency are presented in Fig. 7.

Following the implementation of PS (BW or SRPCP), relative $PSDFRD(f_x)$ values decrease across most spatial frequencies. However, a pronounced increase occurs within the high-frequency regime (0.050–0.070 μm^{-1}), as shown in Fig. 7(a).

Correspondingly, the relative $I(f_x)$ exhibits enhancement in high-frequency regions (0.050–0.070 μm⁻¹). Furthermore, relative $I(f_x)$ also demonstrates enhancement in the low-frequency (0–0.002 μm⁻¹) range. These shifts indicate energy redistribution toward lower spatial frequencies and improved focal spot uniformity at low frequencies, achieved by introducing high-frequency components via adding PS (BW or SRPCP).

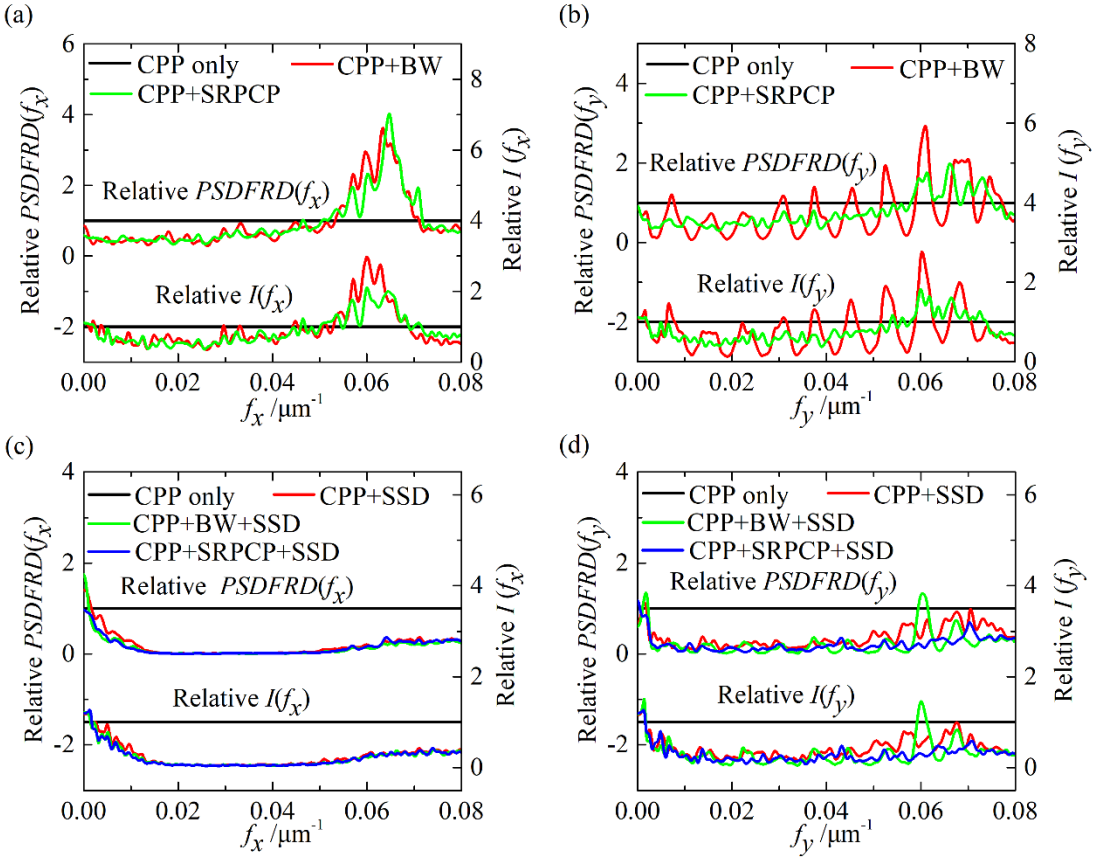


Fig. 7. (colour online) The one-dimensional relative $PSDFRD(f_x)$ (a) and $PSDFRD(f_y)$ (b) for the CPP-only, CPP+BW, and CPP+SRPCP configurations. Similarly, relative $PSDFRD(f_x)$ (c) and $PSDFRD(f_y)$ (d) for the CPP+SSD, CPP+BW+SSD, and CPP+SRPCP+SSD configurations. The corresponding one-dimensional relative intensity distributions $I(f_x)$ and $I(f_y)$ are also plotted in each figure.

Fig. 7(b) displays the one-dimensional relative $PSDFRD(f_y)$ and $I(f_y)$ for the CPP+BW and CPP+SRPCP configurations. For the CPP+SRPCP configuration, the variation trends of relative $PSDFRD(f_y)$ and $I(f_y)$ are essentially consistent with those of relative $PSDFRD(f_x)$ and $I(f_x)$. This directional agreement across orthogonal f_x and f_y directions further confirms the isotropic smoothing behavior of CPP+SRPCP. For CPP+BW, relative $PSDFRD(f_y)$ and $I(f_y)$ exhibit more pronounced periodic variations: at curve troughs, energy decreases and uniformity increases, while at curve peaks, energy increases and uniformity decreases. These variations differ significantly from those of relative $PSDFRD(f_x)$ and $I(f_x)$. The observed discrepancies between orthogonal directions demonstrate the anisotropic characteristics of CPP+BW smoothing. Consequently, CPP+SRPCP achieves more balanced smoothing effects than CPP+BW across the full spatial frequency domain.

Following the introduction of SSD, a significant reduction in one-dimensional relative *PSDFRD* and *I* is observed across most spatial frequencies, as shown in Fig. 7(c) and (d). Notably, SSD eliminates the *PSDFRD* and *I* enhancement at high frequencies induced by PS (BW or SRPCP). However, within the low-frequency range (0-0.001 μm^{-1}), *I* values for CPP+SSD, CPP+BW+SSD, and CPP+SRPCP+SSD increase significantly compared to CCP-only, accompanied by elevated PSDFRD. This indicates that SSD redistributes focal spot energy toward low spatial frequencies while simultaneously increasing non-uniformity in these regions. Further analysis of combined SSD and PS (BW or SRPCP) applications reveals that CPP+SRPCP+SSD achieves optimal performance: it enhances low-frequency energy distribution while most effectively suppressing low-frequency non-uniformity.

5. Conclusion

We propose a method for evaluating focal spot uniformity using PSDFRD, which corresponds to the spatial frequency distribution of squared focal-spot-intensity contrast. This approach enables assessment of smoothing effects that cannot be adequately distinguished by conventional metrics like contrast and FOPAI. Focal spot intensity distributions were measured for six beam smoothing configurations (CPP only, CPP+BW, CPP+SRPCP, CPP+SSD, CPP+BW+SSD, and CPP+SRPCP+SSD), with uniformity analyzed using the proposed method. Key findings include: (1) PS (BW or SRPCP) enhance intensity distribution and improve uniformity in the low-frequency range (0–0.002 μm^{-1}), but introduce increased intensity and non-uniformity at high frequencies (0.050–0.070 μm^{-1}). SRPCP demonstrates superior uniformity in focal spot smoothing across all spatial frequencies compared to BW, which is limited to one-dimensional smoothing capability. (2) SSD implementation reduces energy distribution and improves uniformity across most frequencies. However, it significantly increases both energy and non-uniformity in the low-frequency region (0-0.001 μm^{-1}). The integration of CPP, PS (BW or SRPCP), and SSD not only mitigates elevated high-frequency intensity and non-uniformity inherent to the CPP+PS (BW or SRPCP) configurations but also reduces low-frequency non-uniformity characteristic of the CPP+SSD configuration. PSDFRD provides a novel approach for evaluating the smoothing effect of focal spots in existing beam smoothing techniques and establishes quantifiable parameter criteria for the future development of beam smoothing technologies.

Acknowledgment

The author gratefully acknowledges Bin Li and Qiang Wang at the Institute of Applied Physics and Computational Mathematics for insightful discussions.

References

1. Ji P, Li D, Su X, Jin Y and Wang B 2025 *Opt. Express* **33** 8610
2. Li M M, Liao Q M and Feng Z X 2025 *Appl. Opt.* **64** 6398
3. Lin Y, Kessler T J and Lawrence G N 1996 *Opt. Lett.* **21** 1703
4. Zhang R, Jia H T, Tian X C, Yuan H Y, Zhu N, Su J Q, Hu D X, Zhu Q H and Zheng W G 2016 *Opt. Laser. Eng.* **85** 38

5. Fusaro A, Collin, Riazuelo G, Loiseau P, Thauvin O and Penninckx D 2024 *Phys. Plasmas* **31** 012110
6. Kang N, Liu H Y, Zhou S L, Zhao Y and Lei A L 2021 *J. Opt. Soc. Am. B* **38** 3567
7. Edgell D, Lees, Shah R, Shvydky A and Turnbull D 2025 *Phys. Plasmas* **32** 102701
8. Moody J D, MacGowan B J, Rothenberg J E, Berger R L, Divol L, Glenzer S H, Kirkwood R K, Williams E A and Young P E 2001 *Phys. Rev. Lett.* **86** 2810
9. Rothenberg J E 2000 *J. Appl. Phys.* **87** 3654
10. Zhang C C, Liao W, Jiang X L, Wang H J, Zeng F, Ni W, Li P, Jiang X D and Zhu Q H 2025 *Matter Radiat. Extremes* **10** 057402
11. Wu H H, Xie Y, Sun X B, Wang H, Yuan Q, Liu B W, Pang H, Wu Y T, Gu H, Huang J S and Geng Z M 2026 *Opt. Laser Technol.* **194** 114456
12. Wang Q, Li Z C, Liu Z J, Gong T, Zhang W S, Xu T, Li B, Li P, Li X, Zheng C Y, Cao L H, Liu X C, Pan K Q, Zhao H, Liu Y G, Deng B, Hou L F, Li Y J, Liu X M, Li Y L, Peng X S, Guan Z Y, Wang Q Q, Che X S, Li S W, Yin Q, Zhang W, Xia L Q, Wang P, Jiang X H, Guo L, Li Q, He M Q, Hao L, Cai H B, Zheng W D, Zou S Y, Yang D, Wang F, Yang J M, Zhang B H, Ding Y K and He X T 2023 *Matter Radiat. Extremes* **8** 055602
13. Abu-Shawareb H, et al. 2024 *Phys. Rev. Lett.* **132** 065102
14. Chen C X, Gong T, Li Z C, Hao L, Liu Y G, Liu X M, Zhao H, Liu Y Y, Pan K Q, Li Q, Li S W, Li Z J, Jin S, Wang F and Yang D 2024 *Matter Radiat. Extremes* **9** 027601
15. Pan K Q, Liu Z J, Qin X L, Li J W, Gong T, Wang Q, Yan J, Li Z C, Yang D, Liu Y G and He X T 2025 *Matter Radiat. Extremes* **10** 057401
16. Wang X B, Chai X X, Li P, Zhang B, Zhu Q H, Tian X C, Wang J, Zong Z Y, Zhou S, Yao K, Li S, Zhao J P, Peng Z T 2025 *Matter Radiat. Extremes* **10** 017401
17. Pan K Q, He X A, Li J W, Yu M H, Xiao C Z, Li X, Liu Y Y, Li Q, Li Z C, Gong T, Li S W, Liu Z J, Hao L, Yang D and He X T 2025 *Eur. Phys. J. Spec. Top.* **234** 821
18. Hao L, Gong T, Huo W Yi, Li Z C, Liu Y Y, Qiu J, Li Q, Zhao H, Pan K Q, Li S W, Hou L F, Liu Y G, Liu X M, Li Y L, Zheng W D, Cao L H, Cai H B, Wang L F, Zhao Y K, Dong Y S, Wang F, Yang D, Yang J M, Zhao Z Q, Zou S Y, Zhu S P and Ding Y K 2025 *Nat. Commun.* **16** 10343
19. Xiao C Z, Pan K Q, Wen H, Gong T, Li Z C, Yan J, Yu J Q and Yang D 2025 *High Power Laser Sci.* **13** e59
20. Moreau J G, Blanchot N, Rousseaux C, Baton S D, Penninckx D, Fusaro A, Loiseau P, Collin R, Riazuelo G, Masson-Laborde P –E, Zou J P, Lancia L, Rouyer C, Maunier C, Ribeyre X, Coic H, Selwa O, Daurios J and Neauport J 2025 *Phys. Plasmas* **32** 032102
21. Gong T, Li Z C, Xu T, Wang Q, Liu Y Y, Pan K Q, Ji Y, Zhang W S, Li B, Liu Z J, Li X, Hao L, Yan R, Zhao H, Liu Y G, Deng B, Liu X M, Li Y L, Peng X S, Guan Z Y, Li S W, Jiang X H, Li Q, Zhang W, Zheng J, Li P, Cai H B, Zou S Y, Dong Y S, Wang F, Yang D, Zhu Q H, Yang J M, Zhao Z Q and Ding Y K 2026 *Matter Radiat. Extremes* **11**, 037403
22. Liu B W, Sun X B, Wang H, Yuan Q, Tian M J Y, Chu D Y and Geng Y C 2024

Opt. Express **32** 11491